DEU FMD 26(78) (2024) 379-388

Dokuz Eylül Üniversitesi Mühendislik Fakültesi Fen ve Mühendislik Dergisi
Dokuz Eylul University Faculty of Engineering Journal of Science and Engineering
Elektronik/Online ISSN: 2547-958X

RESEARCH ARTICLE / ARAŞTIRMA MAKALESI

Inversion of Gravity Anomalies by a Hybrid Metaheuristic Algorithm

Gravite Anomalilerinin Hibrit Metasezgisel Algoritma ile Ters Çözümü

Sanam Hosseinzadeh [1*], Gökhan Göktürkler [2], Seçil Turan-Karaoğlan [2]

[1] The Graduate School of Natural and Applied Sciences, Dokuz Eylül University, İzmir, TÜRKİYE
[2]Department of Geophysical Engineering, Faculty of Engineering, Dokuz Eylül University, İzmir, TÜRKİYE

Corresponding Author / Sorumlu Yazar *: sanam.hosseinzadeh@ogr.deu.edu.tr

Abstract

In this work, we introduce application of a hybrid algorithm (DE/PSO) to estimate the model parameters from residual gravity anomalies due to some simple geometrical bodies. This algorithm combines differential evolution (DE) and particle swarm optimization (PSO). To investigate the performance of the hybrid algorithm, test studies were carried out using synthetic and field data sets. The synthetic data sets include noise-free and noisy synthetic anomalies. Two published gravity anomalies from Cuba and Canada were used as the field data. In the hybrid algorithm, DE and PSO yield [premature] solutions separately and share their best solutions during an iterative process. An openly accessible metaheuristics package (*NMOF*) in R programming environment was used to implement the hybrid algorithm. Through simulations using synthetic anomalies, DE/PSO algorithm was successful to provide improved results. In comparison to the solutions from the single algorithms (DE and PSO), the DE/PSO algorithm shows more effectiveness in terms of accuracy and convergence. The true model parameters of noise-free and noisy synthetic gravity anomalies were recovered well by the hybrid algorithm. The results of inversion for the field examples are characterized by low residual values between the observed gravity anomalies and the calculated ones.

Keywords: *Differential evolution, particle swarm optimization, hybrid metaheuristic, gravity anomaly, geophysics*

Öz

Bu çalışmada, basit geometrik şekilli cisimlerden kaynaklanan rezidüel gravite anomalilerin model parametrelerinin kestirimi için bir hibrit algoritmanın (DE/PSO) uygulaması sunulmaktadır. Bu algoritma, Farksal Evrim (DE) ve Parçacık Sürü Optimizasyonunu (PSO) birleştirmektedir. Hibrit algoritmanın performansını araştırmak için kuramsal ve arazi veri setleri kullanılarak test çalışmaları gerçekleştirilmiştir. Kuramsal veri setleri, gürültüsüz ve gürültülü sentetik anomalileri içermektedir. Arazi verileri ise literatürde yer alan Küba ve Kanada gravite anomalileridir. Hibrit algoritmada, DE ve PSO algoritmaları ayrı ayrı [ilksel] çözümler üreterek tekrarlı bir süreç boyunca en iyi çözümlerini paylaşmaktadır. Hibrit algoritmayı gerçekleştirmek için R programlama ortamında açık erişimli bir metasezgisel paket (*NMOF*) kullanılmıştır. DE/PSO algoritması, kuramsal anomalilerin kullanıldığı simülasyonlarda, iyileştirilmiş sonuçlar sağlamada başarılı olmuştur. Her bir algoritmadan (DE ve PSO) gelen çözümlerle karşılaştırıldığında, DE/PSO algoritmasının, doğruluk ve yakınsama açısından daha etkili olduğu görülmüştür. Gürültüsüz ve gürültülü kuramsal gravite anomalilerinin doğru model parametreleri, hibrit algoritma tarafından daha iyi bir şekilde kestirilmiştir. Arazi örnekleri için ters çözüm sonuçları, gözlenen ve hesaplanan gravite anomalileri arasında düşük hata değerlerine sahiptir.

Anahtar Kelimeler: *Farksal evrim, parçacık sürü optimizasyonu, hibrit metasezgisel, gravite anomalisi, jeofizik*

1. Introduction

Gravity field's variations along the Earth's surface are due to variations of density in the subsurface. Then, gravity anomalies are the result of anomalous density structures. Inversion of gravity anomalies is widely used in geophysics to interpret subsurface structures. In this study, we try to solve a small-scale inversion problem, which interprets residual gravity anomalies due to bodies having simple geometric shapes such as horizontal cylinder, vertical cylinder, and sphere. Derivative-based algorithms have been widely used in the inversion of gravity data. However, some disadvantages are highlighted in the literature for the derivative-based methods. These methods are prone to be trapped in local minima. The results from derivative-based methods strongly depend on the initial model. This means that a good initial model is an essential to reach the global minimum, which is not available in most of the case studies. Recent global search methods (metaheuristics) inspired by nature have been introduced to overcome the drawbacks of the derivative-based methods. Although the considerable computational effort is the most important disadvantage of metaheuristics, these algorithms continue to be preferred for addressing optimization problems. The reason for that is their success to avoid local minima. In addition, these algorithms get to the global minimum without depending on the initial model [1,2,3]. A variety of metaheuristics has been implemented to solve geophysical inverse problems. Some examples in the literature for inversion of gravity anomalies include differential evolution-DE [e.g. 4-6], particle swarm optimization-PSO [e.g. 7,8], very fast simulated annealing-VFSA [e.g. 9], backtracking search optimization-BSO [10], and success-history-based adaptive differential evolution-SHADE [11].

DOI: https://doi.org/10.21205/deufmd.2024267804

Geliş Tarihi / Received: 16.05.2023
Kabul Tarihi / Accepted: 12.10.2023

A wide application of metaheuristics to different optimization problems lead to further studies to develop new strategies for the algorithms' modifications. Hybridization is one of the attempts to improve metaheuristics. Hybridization includes combination of metaheuristics with local search algorithms, or with other metaheuristics. Because the strong aspects of the combined algorithms are magnified while their weak aspects are lessened, hybrid algorithms show a better performance [12-14]. Some recent examples of hybrid algorithms for inverting potential-field anomalies comprised DE and PSO [15,16], PSO and evolution strategies (ES) [17], GA and PSO [18], and genetic-price hybrid algorithm (GPA) proposed by Di Maio et al. [19-21].

According to our survey on the literature, inversion of gravity anomalies has been rarely addressed by DE and PSO hybridization. This study tests a hybrid algorithm called DE/PSO to invert gravity anomalies. Both PSO and DE are well-known and popular algorithms widely used to solve optimization problems. The disadvantage of slow convergence has been reported for PSO [e.g. 22,23] and some studies have reported that DE performance is highly sensitive to control parameters selection [e.g. 24,25]. The DE/PSO hybrid gives an opportunity to exploit both algorithms for more accurate results by minimizing their possible disadvantages.

In the DE/PSO hybrid we used, self-contained DE and PSO search their own spaces while sharing their information in parallel. We executed the DE/PSO hybrid algorithm using a metaheuristics package called *NMOF* [26] applicable in the environment of R programming language [27]. R is an open source released under the terms of the GNU General Public License.

2. The DE/PSO Hybrid Algorithm

DE is a stochastic vector-based metaheuristic algorithm consisting of two phases. The first phase is to initialize a random population. The second phase is to evolve the population through mutation, crossover and selection operations. The second phase repeats and a solution is obtained where a termination criterion (e.g. to reach a certain number of generations) is satisfied. The reader can refer to [28], [29], and [30] for more explanation of the algorithm scheme. DE algorithm has two user-defined control parameters to be optimized: F as the parameter for mutation constant and Cr as the parameter for crossover probability.

PSO first introduced by [31] is inspired by the swarming behavior of birds or fishes as they look for sources of food. The procedure of PSO algorithm can be defined in two main steps: starting with a population of particles with random positions, then the positions of the particles are updated iteratively. The iterative process continues until a pre-defined condition, such as reaching a certain number of generations, is met. PSO is controlled by three parameters: ω (inertia weight) as weighting factor ($0 < \omega < 1$); c_1 and c_2 as cognitive and social scaling factors in the range of [0, 1]. The reader can refer to [31], and [32] for more details related to PSO algorithm.

Following the hybrid algorithm suggested by (15), we used a DE/PSO algorithm in this study. In a similar scheme, our used algorithm starts with two different random populations. DE obtains a [premature] solution after N_{gen}^{DE} number of generations. PSO also obtains its [premature] solution after N_{gen}^{DE} number of generations. At this point, the hybrid algorithm picks the best individual, which is the one with less objective function value, between these two solutions. In each iteration, the best individual enters the next generations of DE and PSO. The optimum solution is the final best individual where the hybrid iteration number meets a user-defined maximum iteration number (It_{max}). All the control parameters of DE (F, and Cr) and PSO (ω, c_1, and c_2) are involved in the hybrid algorithm. In addition, the main parameters that tune the hybrid algorithm are population size (N_{pop}), the number of generations per each algorithm ($N_{gen}^{DE}, N_{gen}^{PSO}$), and It_{max}. The hybrid scheme introduced by [15] exchanges the information of the first generations obtained by DE and PSO. On the other hand, the hybrid algorithm introduced in present study was designed to share the information of Nth generations ($N \geq 2$) obtained by DE and PSO.

The flowchart in Fig. 1 illustrates DE/PSO hybrid algorithm. *i*) The algorithm begins with determination of optimum values for DE, PSO, and DE/PSO including $F, Cr, \omega, c_1, c_2, N_{pop}, N_{gen}^{DE}, N_{gen}^{PSO}$, and It_{max}. *ii*) DE and PSO initialize with different populations (pop_{DE} and pop_{PSO}) of size N_{pop}. *iii*) PSO yields a [premature] solution of $N_{gen}^{PSO}th$ generation. *iv*) DE yields a [premature] solution of $N_{gen}^{DE}th$ th generation. *v*) Solutions obtained from DE and PSO are compared based on OF_{DE} (objective function of DE solution) and OF_{PSO} (objective function of PSO solution). The one with smaller objective function value is determined as the best individual. Then, the best individual is carried to the next generation by updating pop_{DE} or pop_{PSO}. *vi*) The algorithm ends if the iteration number gets to It_{max}. If not, it repeats from step (*iii*). In our coding implementation, PSO and DE run in a serial order. On the other hand, they can be implemented simultaneously by parallel programming tools.

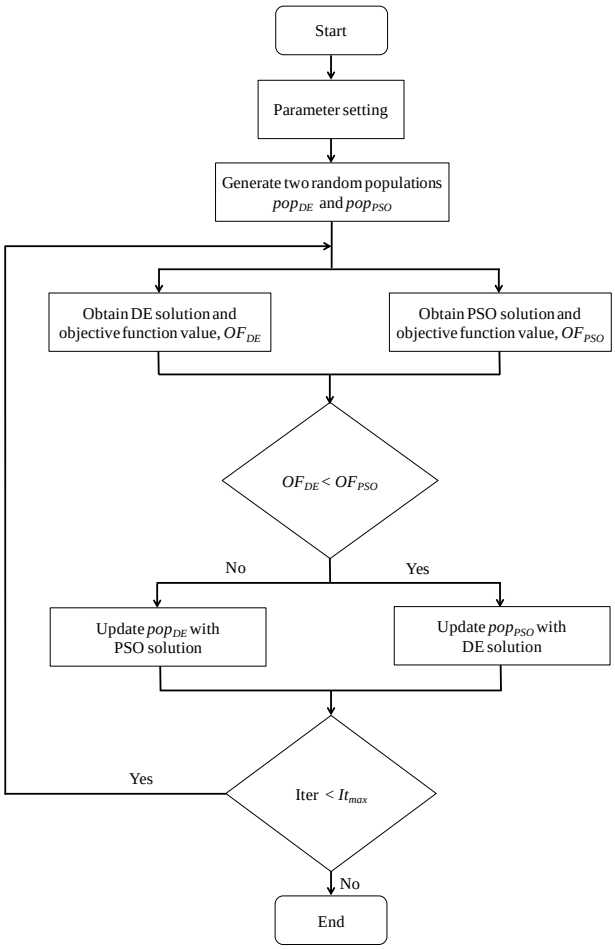

Figure 1. Flowchart of DE/PSO [after 15].

3. Gravity Anomaly

A body in subsurface with a simple geometric shape (sphere, a semi-infinite vertical cylinder or an infinitely long horizontal cylinder) produces gravity anomaly along a profile. At each point of the profile, the following formula gives gravity [mGal] [33,4,34]:

$$g(x, A, z_0, q, \eta, x_0) = A \frac{z_0^{\eta}}{[(x - x_0)^2 + z_0^2]^q} \quad (1)$$

In this equation, x [m] is horizontal distance, A [mGal m$^{2q-\eta}$] is the amplitude coefficient, z_0 [m] and x_0 [m] are the depth of the subsurface body, and its location respectively; and q and η denote dimensionless shape factors. Inversion of gravity anomaly goals to obtain estimations for the model parameters A, z_0, q, η, and x_0. The shape factors (q, η) for a semi-infinite vertical cylinder, infinitely long horizontal cylinder, and sphere respectively are (0.5, 0), (1, 1), and (1.5, 1).

4. Synthetic Data

A gravity profile along 240 m was produced synthetically with points spaced at 2-m intervals using Eq. 1. The subsurface body was assumed as an infinitely long horizontal cylinder with model parameters of A = 250 mGal m, z_0 = 50 m, q = 1, η = 1, and x_0 = 120 m. The gravity anomaly is symmetric and shows a maximum around 5 mGal (Fig. 2). Parameter tunings of DE, PSO, and DE/PSO were carried out using this noise-free synthetic data. Then, we tested DE/PSO hybrid algorithm on noise-free and noisy gravity anomalies. In order to generate a noisy gravity data (Fig. 4), we added pseudo-random numbers with normal distribution having zero mean and standard deviation of ±0.25 mGal [35] to the noise-free gravity data.

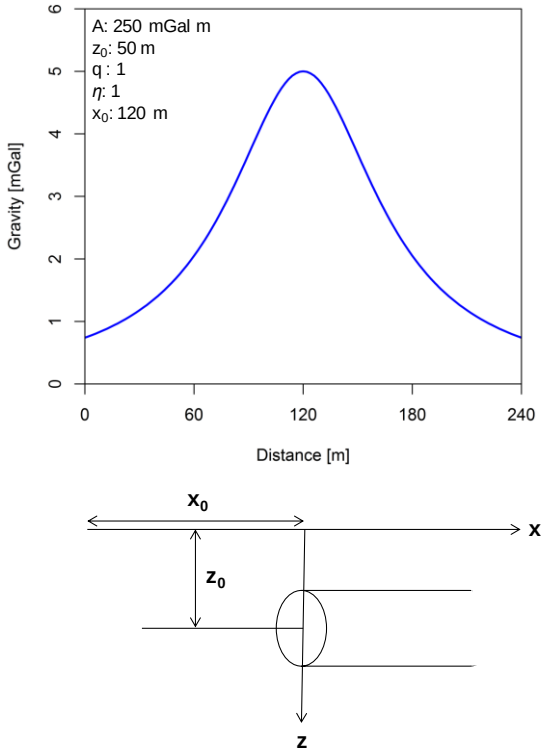

Figure 2. The noise-free synthetic gravity anomaly and the corresponding model parameters for an infinitely long horizontal cylinder.

5. Tuning of DE/PSO Control Parameters

To determine the optimum control parameters involved in the hybrid algorithm, the first step was to tune DE and PSO separately. We implemented each algorithm with fixed population number of 50, and generation number of 100 through synthetic noise-free data set. Each algorithm was executed 10 times, and then the best solution was selected based on the statistical information of the results. The statistical information includes the minimum, maximum, mean, and standard deviation (SD) of root mean square (rms) values, and the mean execution time. It is worth to mention that the parameter tuning, and test studies were implemented in computer with 2.4 GHZ processor and 4 GB of memory. The square root of calculated error energy (E) gives rms value (2):

$$E = \frac{1}{N} \sum_{i=1}^{N} (g_i^{obs} - g_i^{cal})^2 \quad (2)$$

This formula gives error energy for N number of data. For each observation point marked by i, g^{obs} is the observed data (synthetic or field), while g^{cal} is the calculated data.

We considered combinations of F and Cr from [0.4, 0.9] with a step of 0.1 to achieve the optimum for DE control parameters (Table 1). Five different sets of ω, c_1, and c_2 from some previous works were considered to find the optimum for PSO control parameters (Table 2, 3). The optimum control parameters of F, Cr, ω, c_1, and c_2 achieved for DE and PSO were respectively 0.4, 0.9, 0.729, 2.041, and 0.948.

DE/PSO control parameters are N_{pop}, It_{max}, and (N_{gen}^{DE}, N_{gen}^{PSO}). Trial-and-error through the noise-free data set indicated that (N_{gen}^{DE}, N_{gen}^{PSO}) are the most effective parameters that influence the accuracy and the rate of convergence. With fixed N_{pop} of 50, and It_{max} of 100, we obtained the results for several values of 1, 2, 3, and 4 for the parameters (N_{gen}^{DE}, N_{gen}^{PSO}). As we can see in Table 4, the rms and SD values decreases with respect to the increasing (N_{gen}^{DE}, N_{gen}^{PSO}) parameters. The increasing elapsed time is a result of the sequential excution of PSO and DE. It is avoidable with parallel programming approach. The optimum value selected for the parameters (N_{gen}^{DE}, N_{gen}^{PSO}) was 3 as it yielded a satisfactory result in terms of rms, and SD values.

Table 1. Tuning of DE control parameters.

F	Cr	Model Parameters					rms [mGal]				Mean Elapsed Time [s]
		A [mGal.m$^{2q-\eta}$]	z_0 [m]	q	η	x_0 [m]	Min	Max	Mean	SD	
0.4	0.4	248.69	48.30	0.95	0.90	119.93	0.01	0.07	0.04	0.02	0.82
	0.5	296.25	52.24	1.05	1.07	120.01	0.01	0.07	0.04	0.01	0.44
	0.6	255.79	48.66	0.97	0.93	120.06	0.009	0.04	0.02	0.01	0.63
	0.7	278.73	50.07	0.99	0.97	119.98	0.005	0.03	0.02	0.008	0.62
	0.8	271.24	50.04	1.00	0.98	120.00	0.001	0.006	0.003	0.001	0.49
	0.9	**331.92**	**49.98**	**1.00**	**0.93**	**120.00**	**1x10^{-4}**	**7x10^{-4}**	**3x10^{-4}**	**2x10^{-4}**	**0.46**
0.5	0.4	178.34	53.96	1.10	1.31	119.71	0.03	0.09	0.05	0.02	0.47
	0.5	222.67	48.77	0.97	0.96	120.00	0.02	0.08	0.05	0.02	0.65
	0.6	230.87	50.98	1.03	1.09	119.93	0.01	0.06	0.03	0.01	0.47
	0.7	279.82	49.08	0.99	0.94	119.85	0.01	0.03	0.02	0.007	0.60
	0.8	294.30	49.68	1.00	0.94	120.04	0.002	0.02	0.01	0.005	0.64
	0.9	226.84	50.01	1.00	1.02	120.00	2x10^{-4}	0.002	0.001	6x10^{-4}	0.49
0.6	0.4	333.35	49.23	0.97	0.86	119.53	0.03	0.09	0.06	0.02	0.61
	0.5	113.84	44.80	0.91	1.01	119.52	0.05	0.10	0.07	0.02	0.63
	0.6	137.77	50.40	1.00	1.16	120.05	0.01	0.06	0.04	0.02	0.51
	0.7	309.05	47.55	0.94	0.81	119.81	0.02	0.06	0.04	0.02	0.59
	0.8	257.79	50.56	1.00	1.01	119.90	0.006	0.04	0.02	0.01	0.52
	0.9	361.97	49.85	1.00	0.90	120.00	0.004	0.03	0.01	0.008	0.62
0.7	0.4	135.11	50.55	1.01	1.18	120.09	0.01	0.11	0.07	0.02	0.47
	0.5	142.39	46.53	0.92	0.96	120.07	0.03	0.09	0.06	0.01	0.65
	0.6	152.42	48.48	0.96	1.04	120.30	0.02	0.14	0.07	0.03	0.64
	0.7	349.47	49.60	0.97	0.85	119.90	0.02	0.07	0.05	0.01	0.51
	0.8	333.22	50.43	1.01	0.96	120.02	0.009	0.09	0.04	0.02	0.51
	0.9	307.65	51.35	1.03	1.02	119.98	0.01	0.04	0.02	0.01	0.63
0.8	0.4	258.28	47.21	0.94	0.85	120.22	0.04	0.14	0.08	0.03	0.49
	0.5	237.26	54.24	1.05	1.13	120.57	0.06	0.13	0.09	0.02	0.51
	0.6	269.52	57.65	1.16	1.34	118.89	0.06	0.13	0.10	0.02	0.47
	0.7	324.24	49.99	0.98	0.90	119.99	0.02	0.14	0.08	0.03	0.50
	0.8	353.55	48.34	0.98	0.88	119.88	0.04	0.08	0.06	0.01	0.63
	0.9	321.50	49.12	0.97	0.86	120.23	0.02	0.07	0.04	0.01	0.47
0.9	0.4	198.68	44.08	0.88	0.80	119.41	0.06	0.17	0.10	0.03	0.64
	0.5	253.87	58.57	1.15	1.33	120.00	0.07	0.16	0.11	0.02	0.52
	0.6	249.88	55.93	1.17	1.36	119.18	0.05	0.15	0.10	0.03	0.47
	0.7	256.21	45.63	0.87	0.72	119.60	0.06	0.20	0.11	0.05	0.62
	0.8	293.75	56.99	1.20	1.39	120.54	0.05	0.13	0.09	0.02	0.57
	0.9	329.49	50.37	1.00	0.94	120.64	0.03	0.12	0.07	0.03	0.62

Table 2. PSO control parameter sets from some previous studies.

Coefficients	Reference	Inertia Weight	Cognitive Scaling Factor	Social Scaling Factor
Set 1	[31] [42]	1	2	2
Set 2	[43] [44]	0.729	1.494	1.494
Set 3	[45]	0.6	1.7	1.7
Set 4	**[46]**	**0.729**	**2.041**	**0.948**
Set 5	[47]	0.715	1.7	1.7

Table 3. Tuning of PSO control parameters.

Coefficients	Model Parameters					rms [mGal]				Mean Elapsed Time [s]
	A [mGal.m$^{2q-\eta}$]	z_0 [m]	q	η	x_0 [m]	Min	Max	Mean	SD	
Set 1	281.73	46.17	0.85	0.64	21.75	0.11	0.25	0.16	0.05	0.65
Set 2	265.52	50.63	1.02	1.02	119.99	0.005	0.13	0.06	0.05	0.63
Set 3	300.69	52.12	1.05	1.06	120.00	0.01	0.05	0.02	0.01	0.51
Set 4	**224.50**	**50.58**	**1.01**	**1.05**	**120.01**	**0.004**	**0.09**	**0.05**	**0.03**	**0.65**
Set 5	266.57	52.77	1.06	1.13	119.97	0.02	0.13	0.05	0.04	0.52

Table 4. Tuning of DE/PSO hybrid algorithm.

Algorithm	N_{gen}^{DE} / N_{gen}^{PSO}	Model Parameters					rms [mGal]				Mean Elapsed Time [s]
		A [mGal.m$^{2q-\eta}$]	z_0 [m]	q	η	x_0 [m]	Min	Max	Mean	SD	
Hybrid	1	244.43	50.10	1.00	1.01	119.99	8x10^{-5}	0.002	0.0005	0.0006	0.76
	2	244.67	49.99	1.00	1.00	120.00	5x10^{-8}	1x10^{-5}	1 x10^{-6}	3x10^{-6}	1.15
	3	**249.13**	**49.99**	**1.00**	**1.00**	**120.00**	**2x10^{-9}**	**8x10^{-7}**	**1x10^{-7}**	**2x10^{-7}**	**1.48**
	4	237.62	49.99	1.00	1.01	120.00	2x10^{-10}	3x10^{-10}	2x10^{-10}	2x10^{-13}	1.86

6. DE/PSO Hybrid Algorithm Performance

6.1. Synthetic Data

DE/PSO hybrid algorithm was implemented on noise-free and noisy synthetic data sets. For each set of the synthetic data, the algorithm was executed 10 times, and then the best solution was selected based on the rms value of the results. Table 5 includes the estimations with the corresponding rms values, true model parameters, and the search space (determined by trial-and-error). Fig. 3 and 4 show the fit between the observed and calculated gravity anomalies, observed versus calculated data, and the convergence of the error energy. The convergence plots show the first 50 iterations for better resolution. For noise-free data, the estimations are close to true model parameters. For noisy data, the rms value agrees with the standard deviation of the noise, which was added (±0.25 mGal).

Table 5. Test results through synthetic data inversion.

Model Parameters	True Values	Parameter Bounds		Estimated Parameters	
		Minimum	Maximum	Noise-free	Noisy
A [mGal·m$^{2q-\eta}$]	250	50	500	249.13	278.37
z_0 [m]	50	1	150	49.99	51.87
q	1	0	2	1.00	1.04
η	1	0	2	1.00	1.07
x_0 [m]	120	50	200	120.00	119.73
rms [mGal]	-	-	-	1.71x10^{-9}	0.24

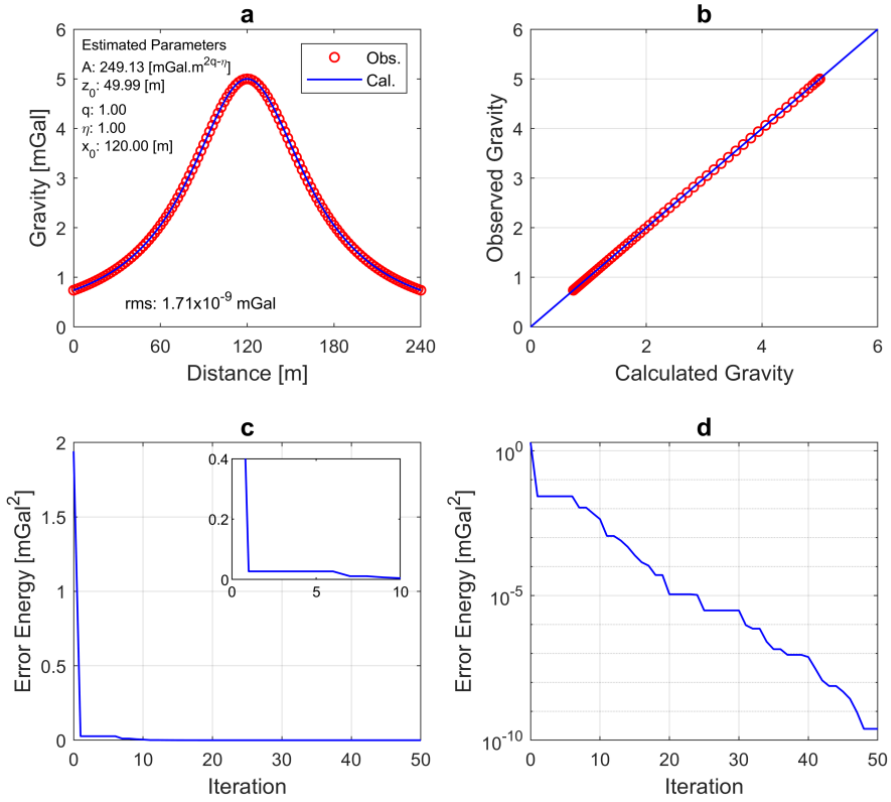

Figure 3. Results from noise-free gravity data including, (a) fit between the observed and calculated data, (b) observed versus calculated data, (c) convergence of the error energy, and (d) convergence of the error energy in logarithmic scale.

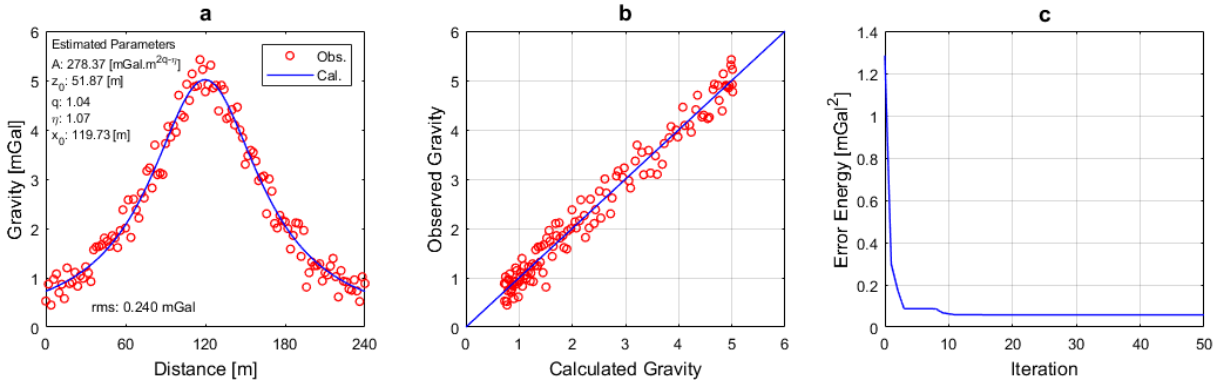

Figure 4. Results from noise-free gravity data including, (a) fit between the observed and calculated data, (b) observed versus calculated data, and (c) convergence of the error energy.

The performance of DE, PSO, and DE/PSO algorithms were compared by using the same parameter values. The value of 100 was assigned for iteration number (It_{max}) and generation number. The three algorithms start with the same initial population size of 50 (Table 6, Fig. 5). According to Table 6, the DE/PSO algorithm yields results with small values of rms and SD in the case of noise-free data. Further investigations to compare the performances of the three algorithms were done through the convergence rate of the three algorithms for noise-free and noisy data. This comparison was based on the necessary iteration/generation numbers for each algorithm to reach the rms value less or equal to 0.01 mGal. The hybrid algorithm requires 19 iterations to reach that threshold rms value, while DE and PSO respectively require 71 and 100 generations.

Table 6. Comparison of DE/PSO, DE, and PSO results through synthetic data inversion.

Synthetic Data	Algorithm	Model Parameters					rms [mGal]				Mean Elapsed Time [s]
		A [mGal.m$^{2q-\eta}$]	z_0 [m]	q	η	x_0 [m]	Min	Max	Mean	SD	
Noise-Free	Hybrid	249.13	49.99	1.00	1.00	120.00	2x10^{-9}	8x10^{-7}	1x10^{-7}	2x10^{-7}	1.48
	DE	241.52	49.93	0.99	1.00	119.98	0.001	0.008	0.003	0.002	0.50
	PSO	231.31	49.29	0.99	0.99	119.95	0.008	0.07	0.04	0.02	0.61
Noisy	Hybrid	278.37	51.87	1.04	1.07	119.73	0.24	0.24	0.24	2x10^{-14}	1.49
	DE	214.94	51.92	1.05	1.14	119.74	0.24	0.24	0.24	1x10^{-10}	0.53
	PSO	220.64	57.29	1.17	1.39	119.95	0.24	0.28	0.25	0.01	0.47

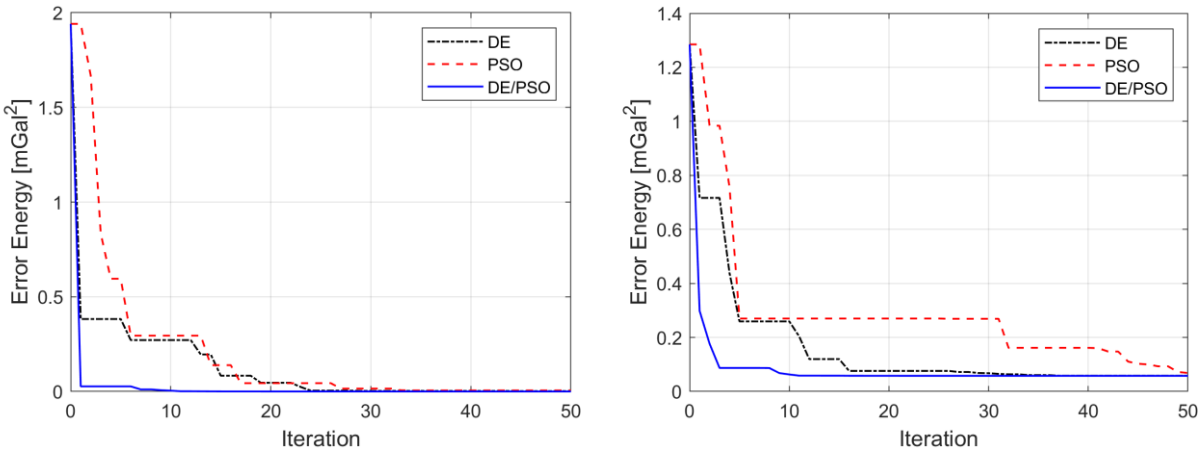

Figure 5. DE/PSO, DE, and PSO convergence rate through noise-free data (left) and noisy data (right) inversion. The plots illustrate 50 iterations for a zoomed-in view of the comparison.

During the test studies, an additional research was done about the success rate of DE and PSO to get the best individual in each iteration of the DE/PSO. According to the investigation, the average success rate of DE and PSO are respectively around %65 and %35 in the test with noise-free data. The values are around %66 and %34 in the test with noisy data.

Prior to inverting the gravity anomalies, error energy maps were generated to examine the solvability of the model parameters addressed in the current inverse problem (36,5,30). Fig. 6 shows the error energy maps for some pairs of the model parameters. Each map is produced by calculating the error energy values (Eq. 2) over the ranges of the associated parameter pair within the search space. Due to the non-uniqueness of the inverse problems, it is acknowledged that there are multiple models that can fit the

data well. Then, the error energy map shows topography that the true model parameters (global minimum) are placed in the location of the lowest error energy value. According to the literature, the shape of contour lines on the topography provides interpretations about the uniqueness in estimating the model parameter. *i*) Closed circular and elliptical contours parallel to any axis (Fig. 6. a-c) represent parameters that are uncorrelated. This suggests that the values of these parameters can be independently obtained. *ii*) Elliptic contours which are angled with one of the axes (Fig. 6. d-f) indicate a correlation between parameters. Despite this correlation, the parameters can still be solved individually. *iii*) Sloping unclosed elliptical contours exhibit a broad region characterized by low errors suggesting the presence of numerous equivalent solutions. This contour shape implies the difficulty in uniquely estimating the related parameters (Fig. 6. g-i). Fig. 6 also shows the locations of the model parameters estimated using the hybrid algorithm for both noise-free and noisy synthetic data. The close proximity of the estimations to the true parameters (global minimum) indicates that the hybrid algorithm has successfully estimated the model parameters.

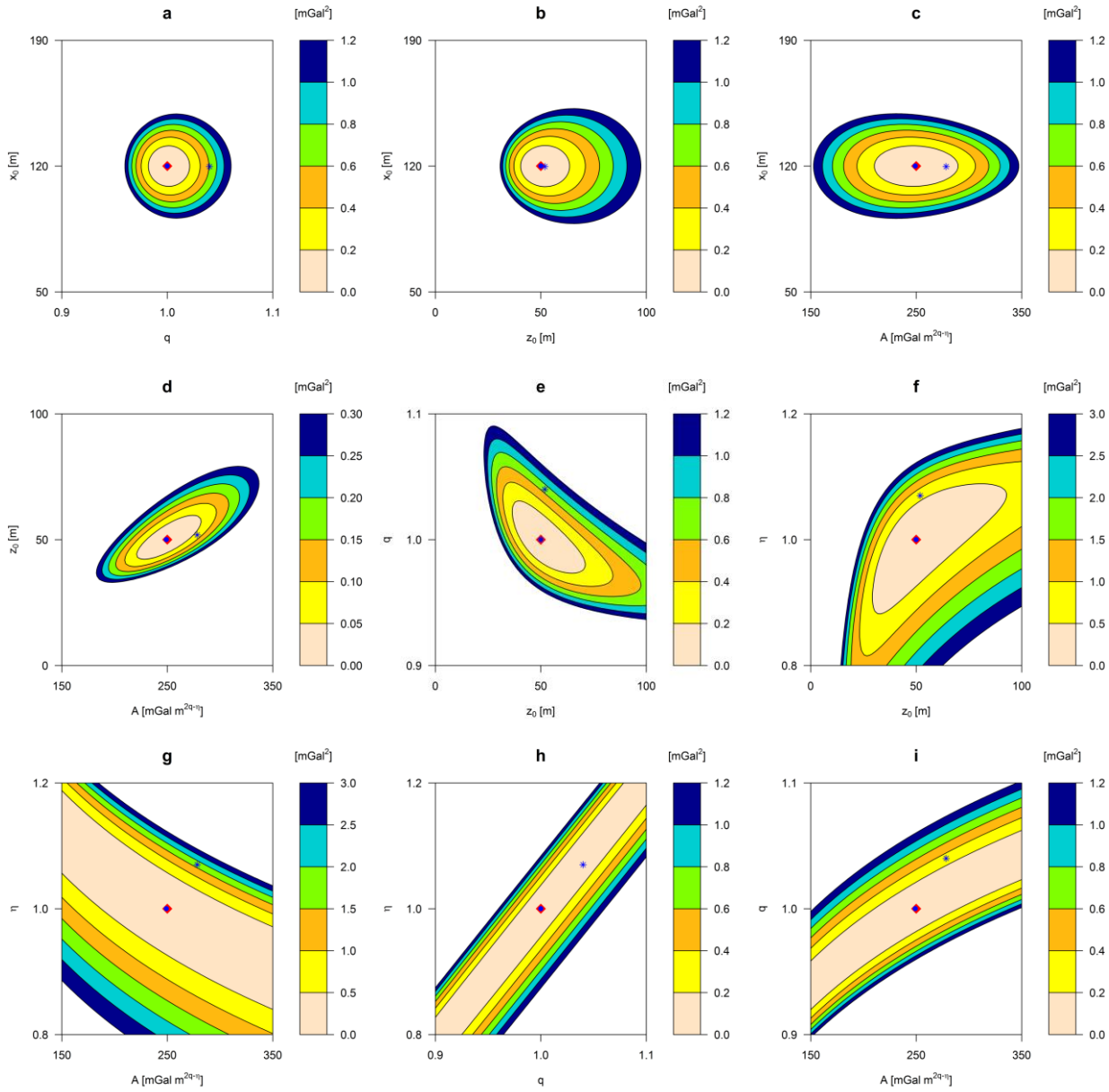

Figure 6. The generated error energy maps for the current inverse problem. The global minimum (red diamond), the model parameters estimated using the DE/PSO algorithm for noise-free (blue circle), and noisy data (blue star) are marked in each map.

6.2. Field Data

In the test with field data, we assigned 200 for N_{pop}, 400 for It_{max}, and 3 for $(N_{gen}^{DE}, N_{gen}^{PSO})$ parameters to obtain the results. These values for the parameters have been chosen based on trial-and-error. The selection of the best solution was carried out similarly to the test with synthetic data, involving 10 independent executions.

6.2.1. Camaguey anomaly (Cuba)

The first data set used as field example was the normalized residual gravity anomaly measured over a chromite deposit in Camaguey province (Cuba) [37]. In Fig. 7, the gravity anomaly is shown along a 120 m profile with a maximum amplitude around 0.2 mGal. We considered the search space following [4,34], except for the q parameter ($A \in [1, 10000]$, $z_0 \in [1, 100]$, $\eta \in [0, 1]$, $x_0 \in$

[0, 120], and $q \in [0, 2]$). Fig. 7 also shows the results estimated by the hybrid algorithm. The convergence plot shows the first 50 iterations for better resolution. Based on the information presented in Table 7, the DE/PSO hybrid algorithm has yielded parameters consistent with those estimated through various methods in prior studies.

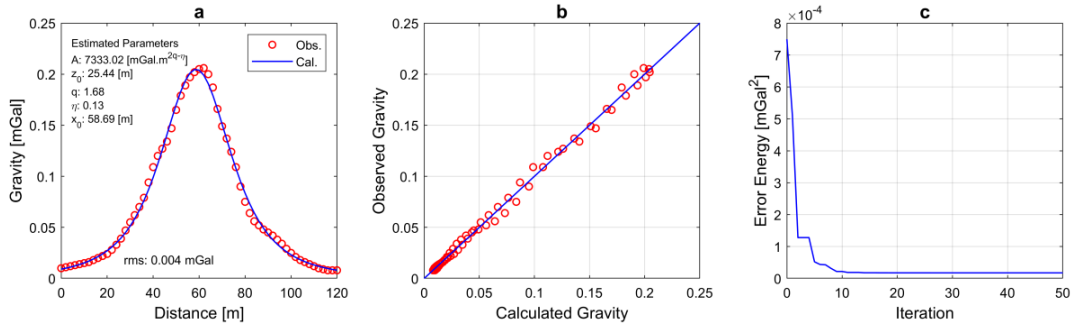

Figure 7. Results from the Cuba anomaly, (a) fit between the observed and calculated data, (b) observed versus calculated data, and (c) convergence of the error energy.

Table 7. Test results through field data (Cuba anomaly) inversion.

Parameters	[38]	[4]	[39]	[34]	[40]	Present Study
	Neural Network	DE	DE	CSA	PSO	DE/PSO
A [mGal·m$^{2q-\eta}$]	9382.52	288.25	175.02	1430.30	408.25	7333.02
z_0 [m]	21.14	23.23	23.23	23.30	21.15	25.44
q	1.54	1.5	1.5	1.49	1.47	1.68
η	-	0.71	0.86	0.18	-	0.13
x_0 [m]	-	58.73	58.73	58.72	0.63	58.69
rms [mGal]	-	0.0043	0.0043	0.00431	0.01	0.0042

6.2.2. Quebec anomaly (Canada)

The second data set used as field example was the normalized residual gravity anomaly measured over a sulfide ore body in Quebec (Canada) [41]. In Fig. 8, the gravity anomaly is shown along a 240 m profile with a maximum amplitude around 1.7 mGal. We considered the search space following [4,34], except for the q parameter ($A \in [1, 10000]$, $z_0 \in [1, 100]$, $\eta \in [0, 1]$, $x_0 \in [0, 240]$, and $q \in [0, 2]$). Fig. 8 also shows the results estimated by the hybrid algorithm. The convergence plot shows the first 50 iterations for better resolution. Based on the information presented in Table 8, the DE/PSO hybrid algorithm has yielded parameters consistent with those estimated through various methods in prior studies.

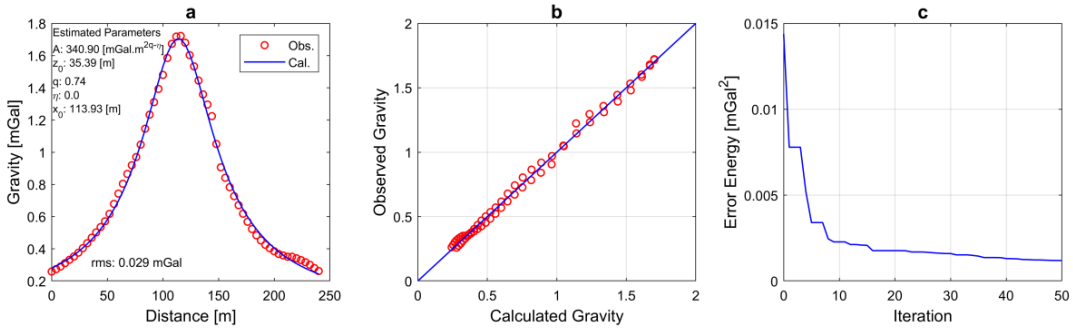

Figure 8. Results from the Canada anomaly including, (a) fit between the observed and calculated data, (b) observed versus calculated data, and (c) convergence of the error energy.

Table 8. Test results through field data (Canada anomaly) inversion.

Parameters	[38]	[4]	[34]	[40]	Present Study
	Neural Network	DE	CSA	PSO	DE/PSO
A [mGal·m$^{2q-\eta}$]	200.11	299.11	204.04	38.51	340.90
z_0 [m]	29.15	35.39	40.32	21.53	35.39
q	0.69	0.74	0.92	0.49	0.74
η	-	0.04	0.23	-	0.002
x_0 [m]	-	113.93	113.66	1.11	113.93
rms [mGal]	-	0.029	0.0334	0.03	0.029

7. Conclusions

In this study, a combination of DE and PSO was applied to gravity anomalies due to some simple geometrical bodies. DE and PSO algorithms were combined as a DE/PSO hybrid algorithm to share their best [premature] solutions in an iterative process. Considering simulations with the synthetic data, the hybrid algorithm successfully obtained results that closely approximated the true model parameters. Compared to DE and PSO, the hybrid algorithm generated results that are more accurate in terms of rms or SD values. The hybrid algorithm also speeded up the convergence rate compared to the ones of DE and PSO. Considering test studies with the field data sets, a good agreement between calculated and observed gravity anomalies from Cuba and Canada indicated that the hybrid algorithm was also successful to obtain the model parameters. Another conclusion worth to mention is the successful applicability of R programming language together with various available R packages to geophysical optimization problems.

Ethics committee approval and conflict of interest statement

This article does not require ethics committee approval.

This article has no conflicts of interest with any individual or institution.

Acknowledgment

As the authors, we are grateful to the Editor and two anonymous reviewers for their comments and suggestions, which contributed significantly to the improvement of the manuscript. The DE/PSO algorithm was performed by using R programming language. MATLAB® software (http://www.mathworks.com/) was also used to create some of the figures. This study is part of the PhD thesis of S. Hosseinzadeh.

Author Contribution Statement

Author 1 (corresponding author) conducted the literature review, wrote the manuscript focusing on conceptualization and results presentation, and developed and implemented the code used in this study. Author 2 supervised the simulation studies, contributed to writing and editing processes, and conducted a critical review offering feedback for improvement. Author 3 contributed to conduct the literature review, provided key insights for the study's theoretical framework, created visual representations, contributed to synthetic dataset generation and editing processes.

References

[1] Blum, C., Roli, A. 2003. Metaheuristics in combinatorial optimization: Overview and conceptual comparison. ACM computing surveys, 35(3), 268-308. https://doi.org/10.1145/937503.937505.

[2] Göktürkler, G. 2011. A hybrid approach for tomographic inversion of crosshole seismic first-arrival times. Journal of Geophysics and Engineering, 8(1), 99-108. https://doi.org/10.1088/1742-2132/8/1/012.

[3] Göktürkler, G., Balkaya, Ç., Ekinci, Y.L., Turan, S. 2016. Metaheuristics in applied geophysics (in Turkish). Pamukkale Univ. Journal of Engineering. Sciences, 22(6), 563–580. https://doi. org/10.5505/pajes.2015.81904.

[4] Ekinci, Y.L., Balkaya, Ç., Göktürkler, G., Turan, S. 2016. Model parameter estimations from residual gravity anomalies due to simple-shaped sources using differential evolution algorithm. Journal of Applied Geophysics. 129, 133-147. https://doi.org/10.1016/j.jappgeo.2016.03.040.

[5] Ekinci, Y.L., Balkaya, Ç., Göktürkler, G., Özyalın, Ş. 2021. Gravity data inversion for the basement relief delineation through global optimization: a case study from the Aegean Graben System, western Anatolia, Turkey. Geophysical Journal International, 224(2), 923-944. https://doi.org/10.1093/gji/ggaa492.

[6] Roy, A., Dubey, P. C., Prasad, M. 2021. Gravity inversion for heterogeneous sedimentary basin with b-spline polynomial approximation using differential evolution algorithm. Geophysics, 86(3), F35–F47. https://doi.org/10.1190/geo2019-0779.1.

[7] Essa, K.S., Mehanee, S.A., Elhussein, M. 2021. Gravity data interpretation by a two-sided fault-like geologic structure using the global particle swarm technique. Physics of the Earth and Planetary Interiors, 311, 106631. https://doi.org/10.1016/j.pepi.2020.106631.

[8] Pallero, J.L.G., Fernandez-Martinez, J.L., Fernandez-Muniz, Z., Bonvalot, S., Gabalda, G., Nalpas, T. 2021. GRAVPSO2D:A matlab package for 2D gravity inversion in sedimentary basins using the Particle Swarm Optimization algorithm. Computers and Geosciences, 146, 104653. https://doi.org/10.1016/j.cageo.2020.104653.

[9] Trivedi, S., Kumar, P., Parija, M.P., Biswas, A. 2020. Global optimization of model parameters from the 2-D analytic signal of gravity and magnetic anomalies over geobodies with idealized structure. In: Biswas, A., Sharma, S. (Eds.), Advances in Modeling and Interpretation in near Surface Geophysics. Springer Geophysics. Springer, Cham, 189–221. https://doi.org/10.1007/978-3-030-28909-6_8.

[10] Ekinci, Y.L., Balkaya, Ç., Göktürkler, G. 2021. Backtracking Search Optimization: A novel global optimization algorithm for the inversion of gravity anomalies. Pure and Applied Geophysics, 178, 4507–4527. https://doi.org/10.1007/s00024-021-02855-3.

[11] Ekinci, Y.L., Balkaya, Ç., Göktürkler, G., Ai, H. 2023. 3D gravity inversion for the basement relief reconstruction through modified success–history–based adaptive differential evolution. Geophysical Journal International, 235(1), 377–400, https://doi.org/10.1093/gji/ggad222.

[12] Blum, C., Puchinger, J., Raidl, G.R., Roli, A. 2011. Hybrid metaheuristics in combinatorial optimization: A survey. Applied Soft Computing, 11(6), 4135-4151. https://doi.org/10.1016/j.asoc.2011.02.032.

[13] Talbi, EG. 2013. A Unified Taxonomy of Hybrid Metaheuristics with Mathematical Programming, Constraint Programming and Machine Learning. In: Talbi EG (ed) Hybrid Metaheuristics. Springer, Berlin, pp 3-76. https://doi.org/10.1007/978-3-642-30671-6_1.

[14] Ting, TO., Yang, XS., Cheng, S., Huang, K. 2015. Hybrid metaheuristic algorithms: past, present, and future. In: Yang XS (ed) Recent Advances in Swarm Intelligence and Evolutionary Computation, Studies in Computational Intelligence. Springer, Berlin, pp 71-83. https://doi.org/10.1007/978-3-319-13826-8_4.

[15] Li, R., Yu, N., Li, R., Zhuang, Q., Zhang, H. 2021. Transient electromagnetic inversion based on particle swarm optimization and differential evolution algorithm. Near Surface Geophysics, 19(1), 59-71. https://doi.org/10.1002/nsg.12129.

[16] Hosseinzadeh, S., Göktürkler, G., Turan-Karaoğlan, S. 2023. Inversion of self-potential data by a hybrid DE/PSO algorithm. Acta Geodaetica et Geophysica, 58, 241–272. https://doi.org/10.1007/s40328-023-00414-x.

[17] Jamasb, A., Motavalli-Anbaran, SH., Ghasemi, K. 2018. A novel hybrid algorithm of particle swarm optimization and evolution strategies for geophysical non-linear inverse problems. Pure and Applied Geophysics, 176(4), 1601-1613. https://doi.org/10.1007/s00024-018-2059-7.

[18] Sohouli, AN., Molhem, H., Zare-Dehnavi, N. 2022. Hybrid PSO-GA algorithm for estimation of magnetic anomaly parameters due to simple geometric structures. Pure and Applied Geophysics, 179, 2231-2254. https://doi.org/10.1007/s00024-022-03048-2.

[19] Di Maio, R., Rani, P., Piegari, E., Milano, M. 2016. Self-potential data inversion through a Genetic-Price algorithm. Computational Geosciences, 94, 86-95. https://doi.org/10.1016/j.cageo.2016.06.005.

[20] Di Maio, R., Piegari, E., Rani, P., Carbonari, R., Vitagliano, E., Milano, L. 2019. Quantitative interpretation of multiple self-potential anomaly sources by a global optimization approach. Journal of Applied Geophysics, 162, 152-163. https://doi.org/10.1016/j.jappgeo.2019.02.004.

[21] Di Maio, R., Milano, L., Piegari, E. 2020. Modeling of magnetic anomalies generated by simple geological structures through Genetic-Price inversion algorithm. Physics of the Earth and Planetary Interiors, 305, 106520. https://doi.org/10.1016/j.pepi.2020.106520.

[22] Sengupta, S., Basak, S., Peters, RA. 2018. Particle Swarm Optimization: A survey of historical and recent developments with hybridization perspectives. Machine Learning and Knowledge Extraction, 1, 157-191. https://doi.org/10.3390/make1010010.

[23] Shami, TM., El-Saleh, AA., Alswaitti, M., Al-Tashi, Q., Summakieh, MA., Mirjalili, S. 2022. Particle swarm optimization: A comprehensive survey. IEEE Access, Vol 10, pp 10031-10061, 2022, https://doi.org/10.1109/ACCESS.2022.3142859.

[24] Eltaeib, T., Mahmood, A. 2018. Differential evolution: A survey and analysis. Applied Sciences, 8, 1945. https://doi.org/10.3390/app8101945.

[25] Salman, A., Engelbrecht, AP., Omran, MG. 2007. Empirical analysis of self-adaptive differential evolution. European Journal of Operational Research, 183, 785-804. https://doi.org/10.1016/j.ejor.2006.10.020.

[26] Gilli, M., Maringer, D., Schumann, E. 2019. Numerical Methods and Optimization in Finance. 2nd edn, Elsevier/Academic Press, Amsterdam.
[27] R Core Team. 2021. R: A language and environment for statistical computing. R Foundation for Statistical Computing, Vienna, Austria. https://www.R-project.org/
[28] Storn, R., Price, K. 1997. Differential Evolution – a simple and efficient heuristic for global optimization over continuous spaces. Journal of Global Optimization, 11, 341-359. https://doi.org/10.1023/A:1008202821328.
[29] Balkaya, Ç. 2013. An implementation of differential evolution algorithm for inversion of geoelectrical data. Journal of Applied Geophysics, 98, 160-175. https://doi.org/10.1016/j.jappgeo.2013.08.019.
[30] Ekinci, Y.L., Balkaya, Ç., Göktürkler, G. 2019. Parameter estimations from gravity and magnetic anomalies due to deep-seated faults: differential evolution versus particle swarm optimization. Turkish Journal of Earth Sciences, 28(6), 860-881. https://doi.org/10.3906/yer-1905-3.
[31] Kennedy, J., Eberhart, R. 1995. Particle swarm optimization. In: International Conference on Neural Networks. IEEE, Piscataway, NJ, USA, November 27- December 1, pp. 1942-1948. https://doi.org/10.1109/ICNN.1995.488968.
[32] Göktürkler, G., Balkaya, Ç. 2012. Inversion of self-potential anomalies caused by simple geometry bodies using global optimization algorithms. Journal of Geophysics and Engineering, 9(5), 498-507. https://doi.org/10.1088/1742-2132/9/5/498.
[33] Abdelrahman, E.M., Bayoumi, A.I., Abdelhady, Y.E., Gobashy, M.M., El-Araby, H.M. 1989. Gravity interpretation using correlation factors between successive least-squares residual anomalies. Geophysics, 54(12), 1614-1621. https://doi.org/10.1190/1.1442629.
[34] Turan Karaoğlan, S., Göktürkler, G. 2022. Gravite Anomalilerinin Guguk Kuşu Arama Algoritması ile Ters Çözümü, Dokuz Eylül Üniversitesi Mühendislik Fakültesi Fen ve Mühendislik Dergisi, 24(72), 799-813. https://doi.org/10.21205/deufmd.2022247210.
[35] Galassi, M., Davies, J., Theiler, J., Gough, B., Jungman, G., Alken, P., Booth, M., Rossi, F. 2009. GNU Scientific Library Reference Manual. 3rd Edn (Bristol: Network Theory Ltd), p. 497.
[36] Fernández-Martínez, JL., Fernández-Muñiz, Z., Pallero, JLG., Pedruelo-González, LM. 2013. From Bayes to Tarantola: new insights to understand uncertainty in inverse problems. Journal of Applied Geophysics, 98:62-72. https://doi.org/10.1016/j.jappgeo.2013.07.005.
[37] Davis, W.E., Jackson, W.H., Richter, D.H. 1957. Gravity prospecting for chromite deposits in Camaguey province, Cuba. Geophysics, 22(4), 848–869. https://doi.org/10.1190/1.1438427.
[38] Al-Garni, M. A. 2013. Inversion of residual gravity anomalies using neural network. Arabian Journal of Geosciences. 6(5), 1509-1516. https://doi.org/10.1007/s12517-011-0452-y.
[39] Ekinci, Y.L., Balkaya, Ç., Göktürkler, G. 2020. Global Optimization of near-surface potential field anomalies through metaheuristics. In: Biswas, A., Sharma, S. (Eds.), Advances in Modeling and Interpretation in Near Surface Geophysics. Springer Geophysics, Springer, pp. 155–188. https://doi.org/10.1007/978-3-030-28909-6_7.
[40] Essa, K.S., Munschy, M. 2019. Gravity data interpretation using the particle swarm optimisation method with application to mineral exploration. Journal of Earth System Science, 128(5), 1-16. https://doi.org/10.1007/s12040-019-1143-4.
[41] Grant, F.S., West, G.F. 1965. Interpretation Theory in Applied Geophysics, New York: McGraw-Hill.
[42] Clerc, M. 1999. The swarm and the queen: towards a deterministic and adaptive particle swarm optimization. In Proceedings of the 1999 congress on evolutionary computation-CEC99 (Cat. No. 99TH8406), IEEE, July 6-9, Vol. 3, pp. 1951-1957. https://doi.org/10.1109/CEC.1999.785513.
[43] Eberhart, R.C., Shi, Y. 2000. Comparing inertia weights and constriction factors in particle swarm optimization. In Proceedings of the 2000 congress on evolutionary computation. CEC00 (Cat. No. 00TH8512), IEEE, July 16-19, Vol. 1, pp. 84-88. http://dx.doi.org/10.1109/CEC.2000.870279.
[44] Clerc, M., Kennedy, J. 2002. The particle swarm-explosion, stability, and convergence in a multidimensional complex space. IEEE Transactions on Evolutionary Computation, 6(1), 58-73. https://doi.org/10.1109/4235.985692.
[45] Trelea, IC. 2003. The particle swarm optimization algorithm: convergence analysis and parameter selection. Information Processing Letters, 85(6), 317-325. https://doi.org/10.1016/S0020-0190(02)00447-7.
[46] Carlisle, A., Dozier, G. 2001. An off-the-shelf PSO. In Proceedings of the Workshop on Particle Swarm Optimization, Indianapolis, IN, USA, pp. 1-6.
[47] Jiang, M., Luo, Y.P., Yang, S.Y. 2007. Stochastic convergence analysis and parameter selection of the standard particle swarm optimization algorithm. Information processing letters, 102(1), 8-16. https://doi.org/10.1016/j.ipl.2006.10.005.